

Contents lists available at ScienceDirect

Journal of the Mechanics and Physics of Solids

journal homepage: www.elsevier.com/locate/jmps





Crystal plasticity modeling of low-cycle fatigue behavior of an Mg-3Al-1Zn alloy based on a model, including twinning and detwinning mechanisms

Xiaoqian Guo ^{a,b,1}, Yao Cheng ^{c,1}, Yunchang Xin ^{c,*}, Wei Wu ^d, Chao Ma ^e, Ke An ^f, Peter K. Liaw ^d, Peidong Wu ^g, Qing Liu ^c

- ^a State Key Laboratory for Geomechanics and Deep Underground Engineering, China University of Mining and Technology, Xuzhou, Jiangsu 221116, China
- b School of Mechanics and Civil Engineering, China University of Mining and Technology, Xuzhou, Jiangsu 221116, China
- ^c Key Laboratory for Light-Weight Materials, Nanjing Tech University, Nanjing, Jiangsu 210009, China
- ^d Department of Materials Science and Engineering, The University of Tennessee, Knoxville TN37996, USA
- ^e School of Physics and New Energy, Xuzhou University of Technology, Xuzhou 221000, China
- f Chemical and Engineering Materials Division, Oak Ridge National Laboratory, Oak Ridge TN37831, USA
- g Department of Mechanical Engineering, McMaster University, Hamilton, Ontario L8S 4L7, Canada

ARTICLE INFO

Keywords: Mg alloys Fatigue Modeling Crystal plasticity Twinning

ABSTRACT

The low-cycle fatigue of strongly-textured Mg alloys is dominated mainly by an alternation of twinning-detwinning process, which poses a great challenge to conventional constitutive models. As a result, a good reproduction of both mechanical response and deformation behavior often fails in previous simulations, in particular for high strain amplitudes. In the present study, the numerical simulations of low-cycle fatigue behavior of an Mg AZ31 plate with $a\pm2\%$ axial strain amplitude along the rolling direction were conducted, using a modified crystal-plasticity based on the finite strain elastic-viscoplastic self-consistent model containing twinning and detwinning mechanisms (EVPSC-TDT), and the results were compared with the mechanical response and deformation behavior determined by a real-time in-situ neutron diffraction. The simulations well predict the hysteresis loops and cyclic-hardening responses throughout the whole fatigue life (80 cycles), along with the evolution of the maximum twin volume fraction and residual twins. For the first time, the evolution of lattice strain throughout the whole fatigue life was calculated, and the results are in good accordance with that determined by neutron diffraction. The present study strongly demonstrates that the EVPSC-TDT model is very effective for modeling the low-cycle fatigue behavior of Mg alloys. More details about the evolution of the maximum twin volume fraction with fatigue cycles are found, an increase from 1st to 2nd cycle, followed by a decrease from 2nd to 20th cycle and a secondary increase after 20th cycle. This finding corrects the previous opinion that the maximum twin volume fraction increases at the initial stage and tends to be saturated at the late stage. Combining the results of simulations and neutron diffractions, the corresponding reasons are explained. Afterward, the mechanisms of the cyclic-hardening behavior at tension stage and compression stage are revisited, and some new insights are provided.

^{*} Corresponding author.

E-mail address: ycxin@cqu.edu.cn (Y. Xin).

¹ These authors contributed equally to this work.

1. Introduction

Magnesium (Mg) and its alloys are promising weight-saving materials for automobile and aircraft industries due to their low density (Kulekci, 2008; Wu et al., 2015; Kang and Li, 2021). The structural components of Mg alloys used in the automobiles, trains, and air planes are frequently subjected to a cyclic deformation (Wu et al., 2010a; Wang et al., 2020), and it is of great importance to investigate fatigue behaviors. Similar to face-centered-cubic (fcc) and body-centered-cubic (bcc) materials, the fatigue deformation of hexagonal-close-packed (hcp)-structured wrought Mg alloys is dominated by dislocation slip under low strain amplitudes. However, at high strain amplitudes, the main deformation mechanism is an alternation of $\{10\overline{1}2\}$ twinning and detwinning during each cycle (Yu et al., 2012). The {1012} twinning with a low critical resolved shear stress (CRSS) can be the predominant mode for plastic deformations at room temperature in highly-textured products, i.e., compression along the rolling direction (RD) of a hot-rolled Mg plate (Knezevic et al., 2010; Dong et al., 2015; Mokdad and Chen, 2015). The $\{10\overline{1}2\}$ twinning generates a lattice rotation of approximately 86° in the twinned region, and the orientation of twins favors detwinning under a reverse reloading (Zhang et al., 2011; Karparvarfard et al., 2019, Zhang et al., 2019). Many in-situ or ex-situ techniques, such as neutron diffraction and acoustic emission, have evidenced this twinning-detwinning behavior (Hong et al., 2011; Kwon et al., 2011; Song et al., 2017; Murphy-Leonard et al., 2019; Zhang et al., 2021b). When detwinning approaches exhaustion, materials will exhibit an elastic behavior and a subsequent deformation by dislocation slip. Therefore, the alternation of twinning-detwinning process is also accompanied by dislocation slip, which develops asymmetrical hysteresis loops (Koike et al., 2010; Kwon et al., 2011). It is reported that the fraction of residual twins increases with fatigue cycles (Yin et al., 2008b). The twin-boundary cracking due to the interactions between twin boundaries and dislocations is considered to be the key reason for the crack initiation of fatigue. Nevertheless, a quantitative investigation on the role of deformation modes in fatigue behavior often fails through experiments.

Numerical modeling is a power tool for quantitatively understanding the mechanisms of fatigue behavior (Zhang et al., 2021a). There have been some simulations addressing the fatigue behavior of Mg alloys. The complicated plastic-deformation behavior of Mg alloys during fatigue loading, in particular the alternation twinning-detwinning process, poses a great challenge to conventional constitutive models. Two types of methods, namely a phenomenological-continuum-plasticity approach and a crystal-plasticity approach, have been adopted. However, in a continuum-plasticity model, materials are considered as a plasticity-deforming homogeneous one, neglecting the underlying deformation mechanisms, dislocation substructure, and other crystallographic features. As a result, the evolutions of slips, twinning, detwinning, and texture cannot be predicted. Crystal-plasticity-based modeling, which is used to account for the behavior and mechanisms of plasticity deformation, is the most frequently-used approach. A full-field approach, crystal-plasticity finite-element (CPFE) containing twinning and detwinning model, has been applied to investigate cyclic deformation behavior of Mg alloys (Chen et al., 2018; Briffod et al., 2019,2020; Zhang et al., 2019; Singh et al., 2020). However, those models often fail to predict the reorientation of multiple twinning variants and account for the deformation mechanisms within these twins. To overcome this problem, a multi-scale CPFE framework, including a physically-based twinning-detwinning model, was proposed by Yaghoobi et al. (2020). The model can reproduce the cyclic response of an Mg ZK60 extruded bar. However, the effect of stress inside the twin on slip, twinning, and detwinning are not included in those CPFE models.

Mean-field plasticity models are also widely used to simulate the plastic deformation behavior of Mg alloys (Lei et al., 2022; Li et al., 2020, 2022). A crystal-plasticity model developed by Guillemer et al. (2011) has been used to model the cyclic-loading behavior of an extruded pure magnesium at small strain amplitudes. The numerical results indicate that this model can successfully reproduce the convex curvature of the curves, while there are still some deviations in cyclic curves and twin volume fractions, especially at higher strain amplitudes. In addition, this model cannot be applied to cyclic loading behavior at large strain amplitudes. A Taylor-Lin elastic-viscoplastic polycrystal model was also applied to model compression-compression fatigue behavior of an AZ31 alloy (Gu and Toth, 2012; Gu et al., 2014). The cyclic stress-strain curves after 500 cycles and the activity of twinning are predicted, but there still exist some deviations in the curves, and the total strain amplitude is only 0.45%. Yu et al. (2014) have developed a model to simulate the uniaxial ratchetting of an Mg alloy under deformations dominated individually by slip or twinning, but the cyclic behavior cannot be reproduced by their model due to a lack of considering the interactions between slip and twinning. More recently, Li et al. (2020) developed a model containing the slip, twinning, detwinning, and back stress effect. The new model can reproduce the uniaxial ratchetting responses which are associated individually with slip or twinning and detwinning, but the evolution of uniaxial ratchetting that is dominated simultaneously by slip, twinning, and detwinning cannot be well predicted. They pointed out that the model was constructed in the framework of small deformation plasticity due to a relatively small final plastic strain, not larger than 10%. As a result, the evolution of texture and its influence on plastic deformation cannot be included. In fact, for large number of cycles, the accumulated plasticity strain is high, therefore, the crystal models valid at small strains will not work. Hence, a crystal-plasticity model containing a large deformation framework and considering slip, twinning, and detwinning is necessary for modeling the low-cycle fatigue behavior of Mg alloys. Recently, a crystal-plasticity model, based on finite strain elastic-viscoplastic self-consistent model, containing twinning and detwinning mechanisms (EVPSC-TDT) was developed by Wang et al. (2010b), to numerically investigate the twinning and detwinning behavior of hcp metallic materials under large strain deformation (Wang et al., 2012a; Wu et al., 2014; Qiao et al., 2015b). It has been demonstrated that the EVPSC-TDT model is a completely general elastic-viscoplastic, fully anisotropic, self-consistent polycrystal model, applicable to large strains and to any crystal symmetry (Wang et al., 2010b). The EVPSC-TDT model and its extended versions have been applied to study the plastic-deformation behavior of hcp materials under various loading conditions, such as monotonic loading, reverse loading, strain-patch change, and cyclic loading (Wu et al., 2014; Guo et al., 2015; Qiao et al., 2015a; Wang et al., 2015a, 2015b; Ma et al., 2017; Qiao et al., 2017b; Ma et al., 2019; Zhao et al., 2019). The simulation results show that the EVPSC-TDT model could capture the stress-strain responses during various loading conditions, and predict well the evolutions of twinning behavior. Hence, this model has potential while has not yet been applied to the fatigue behavior of Mg alloys.

Here we employed the EVPSC-TDT model to simulate the low-cycle fatigue behavior of an AZ31 Mg alloy with $a \pm 2\%$ axial strain amplitude along the RD. The validity of the model was checked by comparing with the experimental results, such as the strain-stress curves, peak stresses, and twinning volume fractions. In addition, the lattice strains from *in-situ* neutron-diffraction measurements in different cycles were also predicted for the first time to further verify the applicability of the EVPSC-TDT model. Afterward, the deformation behavior and the relationship between mechanical response and deformation behavior during fatigue loading were discussed and revisited.

2. Experimental procedures

2.1. Materials and mechanical tests

An Mg AZ31 hot-rolled plate with a strong basal texture (Fig. 1) was used in the present study. The specimens for low-cycle fatigue tests were dog-bone-shaped cylinders with a diameter of 8 mm and a gage length of 16 mm. The low-cycle fatigue tests were carried out at room temperature at a strain amplitude of \pm 2% along the RD using triangular loading waveforms and a frequency of 1 Hz. Before fatigue tests, all specimens were kept in Muffle furnace at 345 °C for 2 h to remove the residual stress generated during sample preparation. *In-situ* neutron-diffraction measurements were conducted during cyclic loading using a VULCAN Engineering Materials Diffractometer and the Spallation Neutron Source (SNS) (Wang et al., 2006). A servo-hydraulic loading system was aligned at a 45° with respect to the incident beam. Two detectors were fixed at \pm 90° with respect to the incident beam, which allows for the collections of diffraction patterns with scattering vectors parallel and transverse to the loading axis, respectively. The full diffraction patterns were recorded using a time-of-flight method. The neutron data were collected continuously throughout all the testing time using 10 min. count time. More experimental details can be found elsewhere (Wu et al., 2010a).

2.2. EVPSC-TDT model

The EVPSC-TDT model developed by incorporating the twinning and detwinning (TDT) scheme into the finite strain EVPSC model (Wang et al., 2012b, 2013), was used to investigate the deformation behavior of an AZ31 Mg alloy during low-cycle fatigue loading. In this section, the constitutive models and equations in the EVPSC-TDT model are briefly introduced. More details about the EVPSC-TDT model can be found in references by Wang et al. (2012b, 2013). In this model, the plastic deformation of a crystal is assumed to be accommodated by a slip and/or twinning system (s^{α}, n^{α}) . Here, n^{α} and s^{α} refer to the slip/twinning plane normal and the slip/twinning direction for a system α , respectively. For Mg alloys, the basal slip $(\{0001\}\langle 11\overline{2}0\rangle)$, extension twinning $\{10\overline{1}2\}\langle \overline{1}011\rangle$, prismatic slip $(\{10\overline{1}0\}\langle 11\overline{2}0\rangle)$, and pyramidal $\langle c+a\rangle$ slip $(\{\overline{11}22\}\langle \overline{11}23\rangle)$ are considered. The plastic-strain-rate tensor for the crystal is given by:

$$d^{p} = \sum_{\alpha} \dot{\gamma}^{\alpha} P^{\alpha} \tag{1}$$

Where $\dot{\gamma}^a$ is the shear rate and $P^a = (s^a n^a + n^a s^a)/2$ is the Schmid tensor for the system α . The driving force for both slip and twinning is the resolved shear stress (RSS), $\tau^a = \sigma : P^a$, where σ is the Cauchy stress tensor. The plastic shear rate $\dot{\gamma}^a$ on the slip/twinning is associated with RSS in terms of the following rate-dependent power-law constitutive formula:

$$\dot{\gamma}^{\alpha} = \dot{\gamma}_0 \left| \frac{\tau^{\alpha}}{\tau_{\rm cr}^a} \right|^{1/m} sgn(\tau^{\alpha}) \tag{2}$$

Where $\dot{\gamma}_0$ denotes the reference shear rate, $\tau_{\rm cr}^a$ is the critical resolved shear stress (CRSS), and m is the strain-rate sensitivity. Due to the polar nature of twinning /detwinning, Eq. (2) is valid for twinning / detwinning only when the RSS is in right direction, otherwise, the shear strain rate is zero.

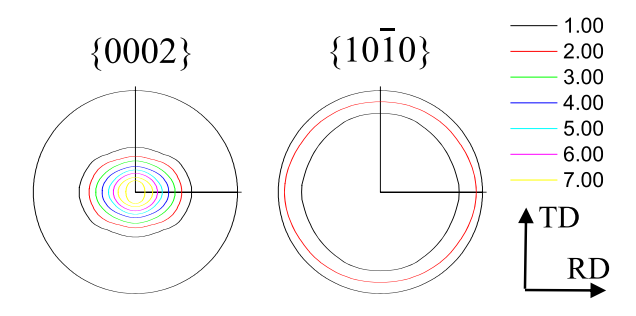


Fig. 1. $\{0002\}$ and $\{10\overline{1}0\}$ pole figures of the Mg AZ31 hot-rolled plate.

In the TDT model, twinning and detwinning can be operated by twin nucleation (Operation A), twin growth (Operation B), twin shrinkage (Operation C), and re-twinning (Operation D). Twin nucleation generates a new twin in a grain free of twin when the RSS in the matrix reaches the CRSS for the operation A (τ_A). Afterward, the grain is divided into a domain of matrix and a domain of twins. The twin expansion can proceed by twin nucleation and/or twin growth, which will increase the volume fraction of twins. Detwinning can be operated through twin shrinkage and re-twinning. Re-twinning refers to the nucleation of twin within a twin, and the twin shrinkage is a reverse process of twin growth. The selected twin variant during re-twinning might be the same variant or a different variant from the pre-existing one. The volume fraction of twins will decrease when Operations C and D are activated. Here, the same with Qiao's simulation work of an Mg alloy ZK60A under cyclic loading (Qiao et al., 2015a), we assume $\tau_A > \tau_B = \tau_C = \tau_D$, and no difference is made between Operations C and D in the present model. It is worth to mention that a TDT model which incorporates secondary twinning is established by Qiao et al. (2017a), but this model is not used in current study.

The net evolution of twin volume fraction related to the twinning system α in a grain, is given by:

$$\dot{f}^{a} = f^{0} \left(\dot{f}^{aA} + \dot{f}^{aC} \right) + f^{a} \left(\dot{f}^{aB} + \dot{f}^{aD} \right) \tag{3}$$

Where f^0 is the volume fraction of the parent, i.e., $f^0 = 1 - f^{tw} = 1 - \sum_{\alpha} f^{\alpha}$, f^{α} is the volume fraction of a given twinning system α , and the superscripts A, B, C and D indicate Operations A, B, C and D, respectively.

In the TDT model, a threshold for twin volume fraction is defined to prevent a complete twinning in the entirety of a grain, since it is rarely observed experimentally. When the twin volume fraction in a grain reaches the threshold, Vth, twinning will be ceased in this grain. Two variables are introduced, the total accumulated twin fraction, V^{acc} , and effective twinned fraction, V^{eff} . It is worth mentioning that V^{acc} and V^{eff} correspond to the weighted volume fraction of the twinned region and volume fraction of grains, in which twinning have been ceased, respectively. The threshold volume fraction, Vth, is defined as:

$$V^{\text{th}} = \min\left(1.0, A_1 + A_2 \frac{V^{\text{eff}}}{V^{\text{acc}}}\right)$$
 (4)

Where A_1 and A_2 are two material constants. Although it is not adopted in the present paper, a EVPSC-TDT model with a single parameter has been recently developed (Qiao et al., 2016b).

In addition, we assume that detwinning could be activated only after twins are formed in grains and when the volume fraction of twins, f_g^{tw} , is larger than a threshold volume fraction of residual twinning, f_{thres} , for the twin ($f_g^{tw} > f_{thres}$). Different from the detwinning control in the original TDT model, here, a new equation describing the residual twins, which is related to the formed twins during previous loading, is proposed as follows,

$$f_{\text{thres}} = \max\left(tiny, \ a \cdot f_{\max,g}^{\text{pre}}\right)$$
 (5)

Where tiny is a small value, being 0.005 here, to guarantee the minimum value of f_{thres} , indicating that the formed twins have a chance to be almost completely detwinned during the reversal loading, and $f_{max,g}^{pre}$, is the maximum volume fraction of twins in a grain formed in previous loadings, while a is a constant to control the residual twinning, in some sense indicating the proportion of residual twinning in previous formed twins. It should be pointed that the maximum twin volume fraction f_{max}^{pre} formed in previous loading may vary, so the f_{thres} may be different, rather than a constant value for all grains.

The CRSS, τ_{cr}^{α} for both slip and twinning is calculated by:

$$\dot{\tau}_{\rm cr}^{\alpha} = \frac{d\hat{\tau}^{\alpha}}{d\Gamma} \sum_{\beta} h^{\alpha\beta} |\dot{\gamma}^{\beta}| \tag{6}$$

Where $\Gamma = \sum_{\alpha} \int |\dot{\gamma}^{\alpha}| dt$ represents the accumulated shear strain in the grain, and $h^{\alpha\beta}$ is the latent hardening coupling coefficient, representing the obstacles on the system, α , related to the system, β . $\hat{\tau}^{\alpha}$ is the threshold stress and is characterized by:

$$\widehat{\tau}^{a} = \tau_{0}^{a} + \left(\tau_{1}^{a} + h_{1}^{a}\Gamma\right) \left(1 - \exp\left(\frac{h_{0}^{a}}{\tau_{1}^{a}}\Gamma\right)\right) \tag{7}$$

Here, τ_0 , h_0 , h_1 , and $\tau_0 + \tau_1$ represents the initial CRSS, the initial hardening rate, the asymptotic hardening rate, and the back-extrapolated CRSS, respectively.

It has been demonstrated that the simulated response is very sensitive to the self-consistent scheme employed by Wang et al. (2010b). An examination by applying various self-consistent schemes to a large-strain deformation behavior of an Mg AZ31 plate under different deformation processes shows that the *Affine* self-consistent scheme exhibits the best overall performance (Wang et al., 2010a). Therefore, the *Affine* self-consistent scheme was used in current study.

2.3. Lattice strain

Lattice strains defined as the normalized lattice-plane spacing difference between under load and at zero load can be calculated by the equation below:

$$\left\langle e^{\text{hkls}}\right\rangle = \frac{\left\langle d^{\text{hkls}}\right\rangle - d_0^{\text{hkls}}}{d^{\text{hkls}}}$$
 (8)

Where $\langle e^{hkls} \rangle$ is the lattice strain for a lattice-plane hkls, d_0^{hkls} and $\langle d^{hkls} \rangle$ are the reference interplanar spacings at zero load and under an applied load, respectively. A counting time of 10 min for measuring the reference at zero load was employed to reduce the propagated d_0^{hkls} statistic error (Wu et al., 2014, 2015). The lattice strain mainly results from the Cauchy stress in a subset of grains (Wang et al., 2012a; Qiao et al., 2015a). In the simulation, all grains with the normal vectors falling within a certain angle are added to a subset. A volume-weighted average of the elastic strain parallel to the hkls normal vector over the subset of grains allows for a direct comparison with the lattice strain determined experimentally (Qiao et al., 2015a).

3. Results

3.1. Materials parameters for simulations

A typical basal texture by constructing of 1748 grains from a hot-rolled Mg AZ31 plate was used in simulations. The elastic constants for the magnesium single crystal at room temperature follow those from Simmons and Wang (1971): $C_{11} = 58.0$, $C_{12} = 25.0$, $C_{13} = 20.8$, $C_{33} = 61.2$, and $C_{14} = 16.6$ (units of GPa). $\dot{\gamma}_0 = 0.001~s^{-1}$ and m = 0.05 are prescribed for all slip/twinning systems. The fitting of the experimental stress-strain curves for monotonic uniaxial tension and compression from Wu et al. (2014) is employed to determine the values for hardening parameters (Fig. 2). The monotonic tension and compression tests were carried out at a strain rate of 10^{-4} . The EVPSC-TDT model can reproduce well the experimental curves by the hardening parameters in Table 1. The value of parameter a in Eq. (5) is assumed to be 0.05, which is determined by the curve-fitting of the mechanical response in 1st cycle (especially stage DA', in Fig. 3b).

3.2. Mechanical response

The simulated hysteresis loops (red solid lines) are compared with the experiment ones (black solid square symbols) in Fig. 3. The stress-strain hysteresis loops show an asymmetric shape throughout the whole fatigue life from 1st to 80th cycles, since the hardening is important in positive loading whereas it is quite nil in compression. This trend is consistent with that in previous researches, and this effect is particularly evident for a larger applied plastic strain (Chen et al., 2012; Duan et al., 2014; Murphy-Leonard et al., 2019). Specifically, during reverse compression, the flow curve displays a plateau shape, the typical feature of $\{10\overline{1}2\}$ twinning. The curve for reverse tension stage exhibits a rapid strain hardening of elastic stage, followed by a subsequent steady hardening by detwinning, and a secondary rapid hardening after the exhaustion of detwinning. The hysteresis loops for subsequent cycles has a similar shape to that of the 1st cycle. Evidently, the results in Fig. 3b—h demonstrate that the simulated responses are in a good accordance with the experimental ones. It should be noted that the back stress is not considered in the present model, but the characteristics of the stress-strain response in each cycle are well reproduced by the EVPSC-TDT model with less parameters, compared to the model including a back stress

The evolution of the peak stresses for experiments and simulations as a function of loading cycle are compared in Fig. 4. It is found that the simulation well reproduces the evolution of peak stress with fatigue cycles. It is worth mentioning that the peak stresses at tension stage are much higher than these at compression stage in each cycle. There is a slow increase for the peak stresses at tension stage before the 10th cycle, while a fast increase at compression stage. A much stronger cyclic hardening for the compressive peak stress (61 MPa) than the tensile peak stress (25 MPa) is observed after 80 cycles.

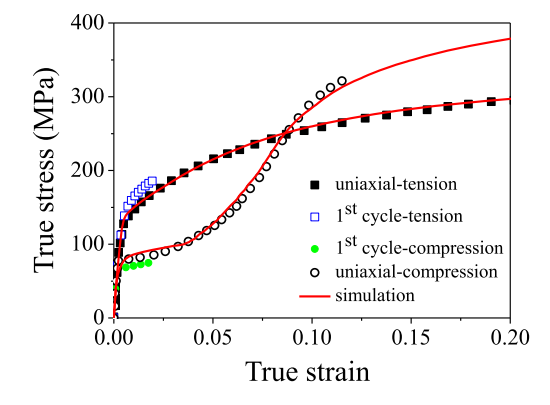


Fig. 2. Experimental and simulated stress-strain curves under monotonic uniaxial tension and compression along the RD of the Mg AZ31 sheet used in the present study.

Table 1Values of material parameters determined by curve-fitting in Fig. 2. The parameter h^{st} denotes the latent hardening effect of the twinning mode t upon other deformation modes. *All other latent hardening parameters are 1*.

Mode	$ au_0(ext{MPa})$	$\tau_1(\text{MPa})$	$h_0(MPa)$	$h_1(MPa)$	$h^{\rm st}$	A_1	A_2
Basal slip	15	1	10	1	1		
Prismatic slip	80	68	500	1	1		
Pyramidal slip	100	155	1400	0	1		
$\{10\overline{1}2\}$ twinning	A(30) B=C=D (18)	40	100	0	1	0.6	0.75

3.3. Microscopic response

3.3.1. Diffraction peak intensity

The evolutions of the diffraction peak intensities for certain hkls along the axial directions in selected fatigue cycles are presented in Fig. 5. As previously mentioned, $\{10\overline{1}2\}$ twinning reorients a twinned region by approximately 86° . Consequently, when the $\{10\overline{1}2\}$ twinning is activated, the intensities of diffraction peak for (0002) grains increase, and those of $(10\overline{1}0)$ decrease simultaneously on the same detector bank. An alternation of the increase–decrease or decrease–increase sequence is observed for $(10\overline{1}0)$, (0002), and $(11\overline{2}0)$ grains. It indicates that twinning and detwinning take place alternatively with a sequential tension–compression loading in each cycle.

It can be seen that the diffraction peak intensities for the (0002) grains in the axial direction at the minimum strain, -0.02, firstly increase, then decrease, and increase again progressively with the increase of fatigue cycles, suggesting that the maximum twin volume fractions increase first, then decrease, and increase again. For cycles 1, 2 and 5, the peak intensities for the (0002) grains are completely recovered. After the 20th cycle, a gradual increase of the peak intensities for the (0002) grains is observed with more cycles. This indicates that the twins generated during compression are completely detwinned during the subsequent tension before the 20th cycle, while an accumulation of residual twins appears after the 20th cycle.

The predicted twin volume fraction as a function of the strain is shown in Fig. 6. The first tension generates a twin volume fraction of approximately 2.5%, and the twin volume fraction reaches approximately 35% after the first compressive strain of - 2%, and then decreases rapidly to 7.5% at the strain of 1.5% during the DA' stage. Evidently, detwinning is exhausted at this point. The detwinning is exhausted at a higher strain with the increase of fatigue cycles. The twin volume factions of other cycles have the same tendency as the first cycle. The maximum twin volume fraction (at Point C) and residual twin-volume fraction (at Point A') are presented in Fig. 7. Two points are worth mentioning. First, the maximum twin volume fraction of each cycle is found: first increases (1st to 2nd cycle), then decreases (2nd to 20th cycle), and increases again (20th to 80th cycle) which reflects the same tendency with the results by neutron diffraction. Second, the twin volume fraction decreases to 7.5%, rather than 0, during the reverse loading to tension at the first cycle, which indicates that the residual twin appears at the first cycle in our simulation. This is different with the experimental observation of the normalized intensity (shown in Fig. 5). The reasons for this trend will be discussed in Section 4.1. In addition, the fraction of residual twins at this point increases gradually with the increase of fatigue cycles.

3.3.2. Evolution of lattice -strains

Fig. 8 shows the measured and predicted lattice strains in the $\{0002\}$, $\{10\overline{1}0\}$, $\{11\overline{2}0\}$, and $\{10\overline{1}1\}$ families along the RD from the 1st to 80th cycle. The results show that the simulations are in reasonable agreement with those determined experimentally in terms of both the trends and magnitudes. For the first cycle, the lattice strains in the $\{10\overline{1}0\}$, $\{11\overline{2}0\}$, and $\{10\overline{1}1\}$ families show a linear increase with the applied stress at the beginning of tension (Stage O to P_A). As reported by Agnew et al. (2006), the non-linearity of lattice strains is related to the activation of the basal slip, which has a relative low CRSS. The final lattice strains at Point A in the $\{10\overline{1}0\}$ and $\{11\overline{2}0\}$ grains are higher than these in other orientation grains. When the specimen is unloaded to 0 MPa after the tension, compressive lattice strains can be seen in the $\{10\overline{1}0\}$, $\{11\overline{2}0\}$, and $\{0001\}$ grains. When the stress is reverse to compression, the $\{11\overline{2}0\}$ grains tend to share more loads than other grains, and the $\{0002\}$ grains have a relatively-small lattice strain. When the specimen is unloaded to 0 MPa after compression, the $\{0002\}$ grains contain a relatively-large tension residual strain. In a reverse tension stage, plastic deformation is mainly accommodated by detwinning and dislocation slip, sequentially. The responses of lattice-strain for different grain groups in each stage are different. During the detwinning predominant deformation, the peak intensity of $\{11\overline{2}0\}$ increases and $\{11\overline{2}0\}$ grains tend to carry more load than others. During the slip predominant deformation, $\{11\overline{2}0\}$ grains start to yield, and $\{10\overline{1}0\}$ and $\{11\overline{2}0\}$ grains receive more load. The general evolution of the lattice-strain for different grain groups in the subsequent cycles is similar to that in the 1st cycle, which suggests that the fatigue cycling hardly affects the load sharing mechanisms for different orientation families.

As described in Section 3.2, with the increase of fatigue cycle, both the tensile and compressive peak stresses increase, leading to the unfixed positions of Points A and C for different cycles. In order to compare the evolution of lattice strain of a certain plane with fatigue cycles, the data are re-plotted as macro-strain vs. micro-strain. Fig. 9 shows the experimental and simulated evolutions of lattice strains in the $\{0002\}$, $\{10\overline{1}0\}$, $\{11\overline{2}0\}$, and $\{10\overline{1}1\}$ families along the RD under different cycles. Note that during the stress reverse to compression, the $\{11\overline{2}0\}$ grains tend to carry larger lattice strains with the increase of fatigue cycles. To the best of our knowledge, it is the first time that the evolution of the experimental lattice-strain under fatigue deformation of Mg alloys is simulated.

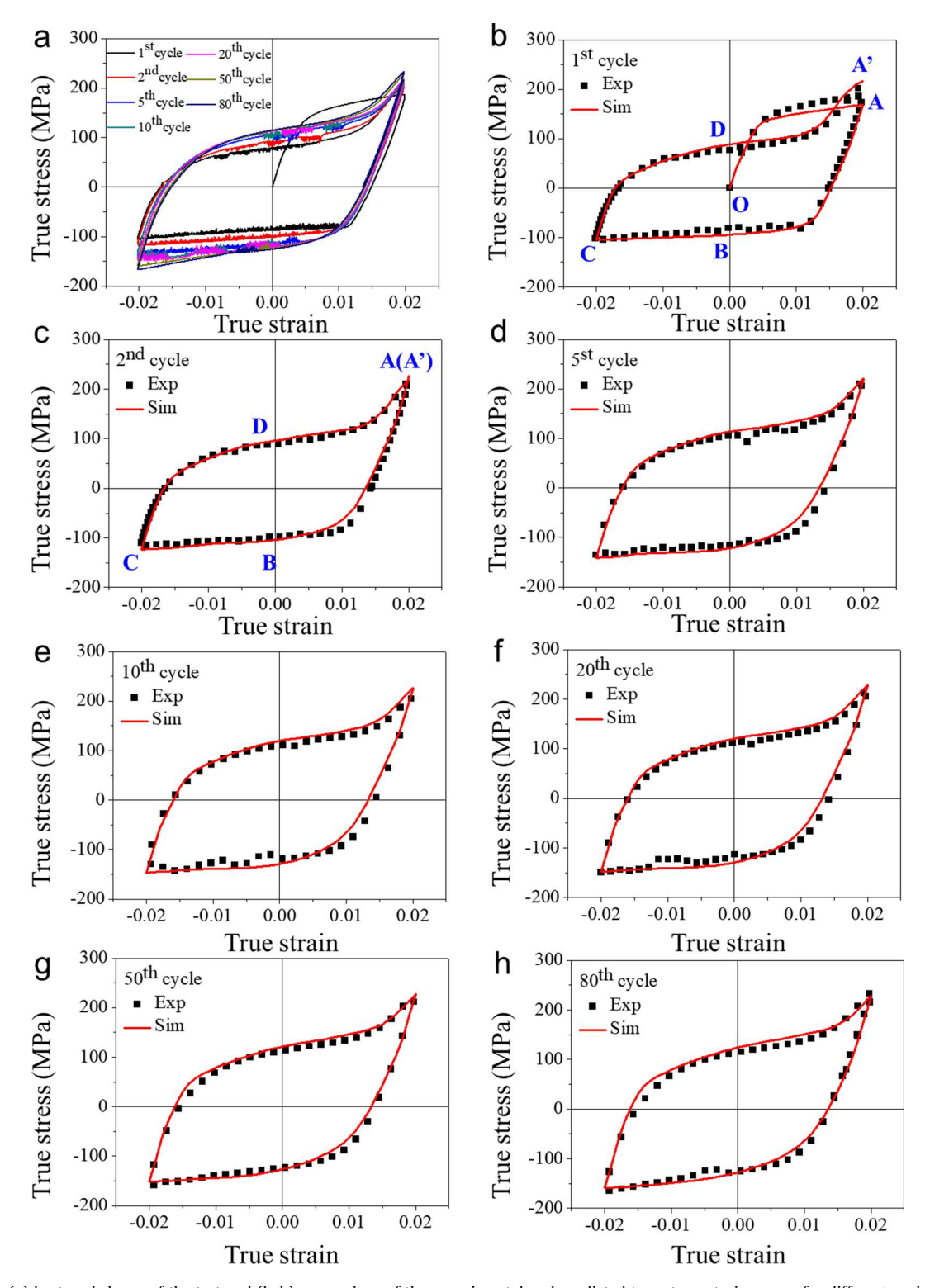


Fig. 3. (a) hysteresis loops of the test and (b-h) comparison of the experimental and predicted true stress-strain curves for different cycles of the AZ31 plate.

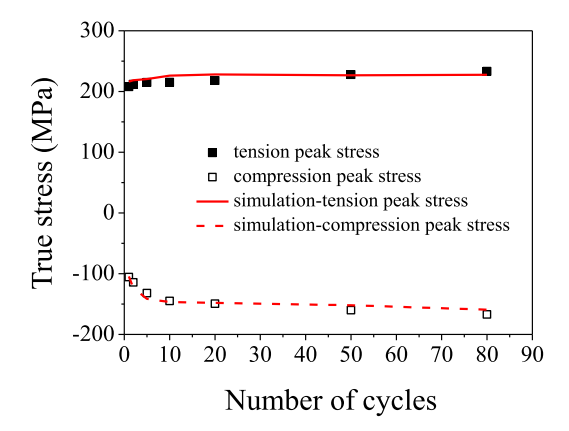


Fig. 4. Maximum tensile and compressive stress amplitudes as a function of fatigue cycle for the AZ31 plate.

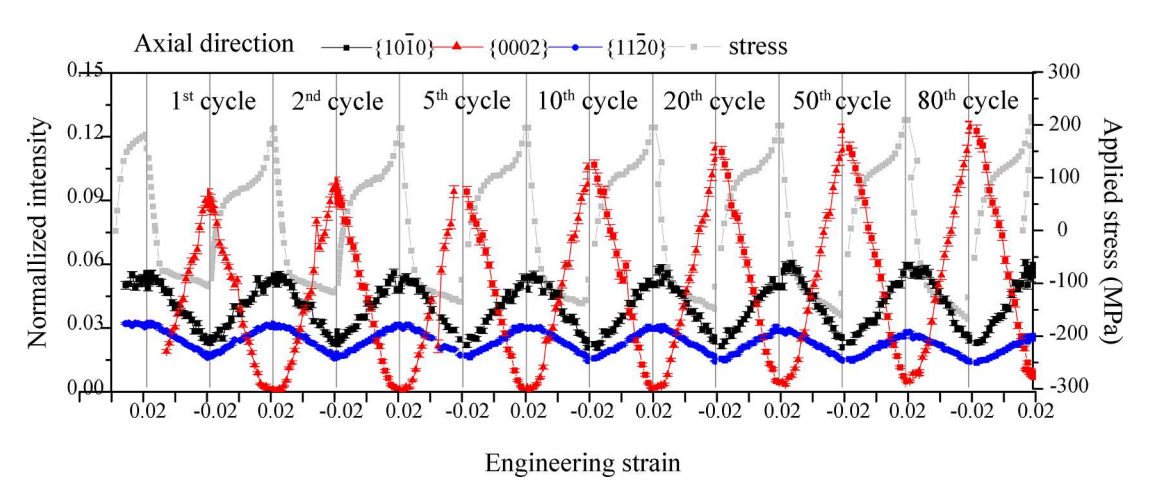


Fig. 5. Evolution of real-time in-situ neutron-diffraction peak intensities at different cycles for the AZ31 plate.

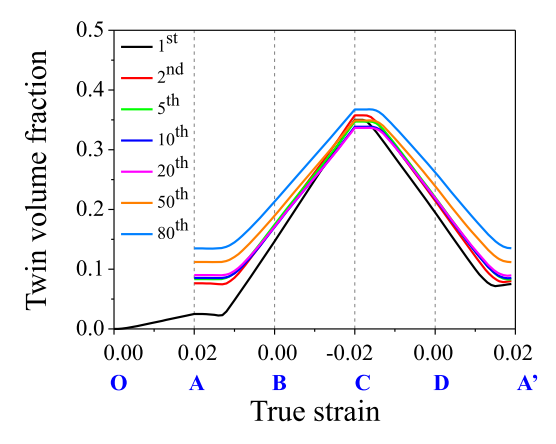


Fig. 6. Predicted twin volume fractions as a function of strain for different fatigue cycles of the AZ31 plate.

3.3.3. Relative activities of deformation modes

The relative activities of different deformation modes at different cycles are plotted in Fig. 10. Take the first cycle as example, the deformation modes for Stage O-A are prismatic and basal slips, and the relative activity of the basal slip is higher than that of the prismatic slip. This trend is in accordance with the previous research that a spread of basal poles along the rolling direction allows the activation of the basal slip under tension along the RD (Agnew et al., 2003). The result of a lower relative activity of twinning is consistent with the prediction of the twin volume fraction in Fig. 6. For the stage of A-C, basal slip and $\{10\overline{12}\}$ twinning are

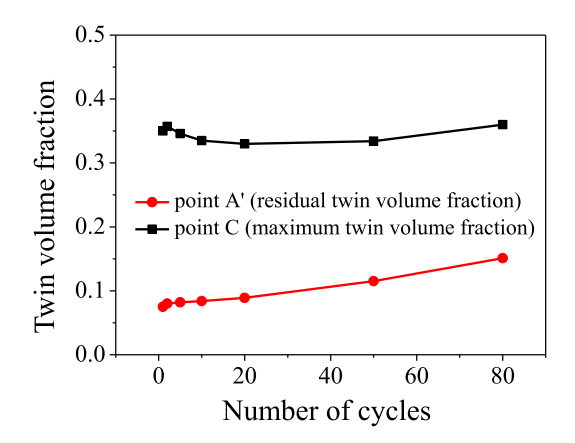


Fig. 7. Predicted twin volume fractions at the point A/A' and C for different cycle for the AZ31 plate.

predominant. The activity of twinning decreases gradually, while that of basal slip increases slowly. The contribution of prismatic slip is very pronounced at the later stage of D-A'. With an increase of strain, basal slip shows a higher relative activity than extension twining from the 5th cycle at the later stage of B, C. The evolution of the relative activities for basal slip, prismatic slip, pyramidal slip and extension twinning with fatigue cycle are plotted in Fig. 11. Significant differences can be noticed. Extension twinning exhibits a decreasing relative activity with cycles, in contrast to an increasing activity for basal slip.

4. Discussion

4.1. Twinning and detwinning as a function of fatigue cycles

Although some crystal-plasticity-based simulations have been conducted to model the low-cycle fatigue behavior of Mg alloys, the results are often not satisfactory. Some simulations cannot even give a good prediction of mechanical response. A part of simulations can well reproduce stress-strain curves, while fail to accurately predict deformation behavior (Guillemer et al., 2011; Gu and Toth, 2012; Gu et al., 2014; Chen et al., 2018; Briffod et al., 2019; Zhang et al., 2019b; Briffod et al., 2019; Singh et al., 2020). The main reason lies in that an alternation of twinning-detwinning during low-cycle fatigue poses a great challenge to constitutive models. Many previous models considering only the predominant twinning system often did not include a detwinning scheme. In the EVPSC-TDT model, both the twinning and detwinning model are included, and all possible twinning variants are considered. As a result, the EVPSC-TDT model is very effective for the simulation of low-cycle fatigue behavior of Mg alloys, as demonstrated in the present study. Previously, the EVPSC-TDT model is widely used in the simulations for uniaxial loading, plain-strain compression, and strain-path change (Wu et al., 2014; Guo et al., 2015; Qiao et al., 2015a; Wang et al., 2015b; Ma et al., 2017; Qiao et al., 2017a, 2017b; Ma et al., 2019; Zhao et al., 2019). The present study is the first time for this model to be applied to simulate the fatigue behavior of Mg alloys.

The alternation of twinning and detwinning is the predominant mode during low-cycle fatigue of highly-textured Mg alloys, and it is closely related to the cyclic hardening and failure process. Three distinctive twinning mechanisms, namely fresh twinning, detwinning and re-twinning, have been reported by Yu et al. (2013) during cyclic loading of a single crystal Mg. Fresh twinning refers to the nucleation and propagation of new twins from the virgin material, and re-twinning corresponds to the repeated growth of a residual twin that is not fully detwinned (Yu et al., 2011, 2013). This behavior will tend to create some permanent shear channels inside the grain. The gliding dislocations due to basal/non-basal slips and residual twin dislocations after repeated twinning-detwinning process can multiply, accumulate, and might be pinned at twin boundaries. Certain irreversible dislocation substructures can stabilize twin boundaries, making the migration of twin boundaries more difficult (Dong et al., 2015, 2017). Those dislocation-twin interactions will result in a cyclic hardening. It is important to point out that Qiao et al. (2017a) have demonstrated that the EVPSC-TDT model is able to predict fresh twinning, detwinning, re-twinning and double twinning occurred simultaneously in a commercial hot-rolled AZ31 Mg alloy subjected to consecutive in-plane compressions along the RD and TD. However, it is also important to mention that spatial inhomogeneities such as the permanent shear channels inside a grain cannot be accounted in the EVPSC-TDT model due to the nature of polycrystal plasticity models. Nevertheless, such an inhomogeneity can be considered by crystal plasticity based finite element (CPFE) using many elements per grain (see e.g. Qiao et al. 2016a).

It is considered that the crack initiation is mainly related to those residual twins, and a higher fraction of residual twins will accelerate fatigue failure (Yu et al., 2011). Previously, the twinning behavior during cyclic loading has been widely investigated and discussed in the literatures (Yin et al., 2008a, 2008b; Park et al., 2010, 2016; Lv et al., 2011a, 2011b). Most experimental studies focus on mainly the first cycle or a certain cycle using *in-situ* or *ex-situ* experimental techniques. As the evolution of twinning and detwinning with fatigue cycle is concluded based on the results of quite limited cycles, some conflicting conclusions have been developed. It is generally considered that the maximum twin volume fraction at each cycle gradually increases and tends to be saturated. Matsuzuki and Horibe (2009) thought that the twinning-detwinning behavior was outwardly saturated in the relatively-early cycles.

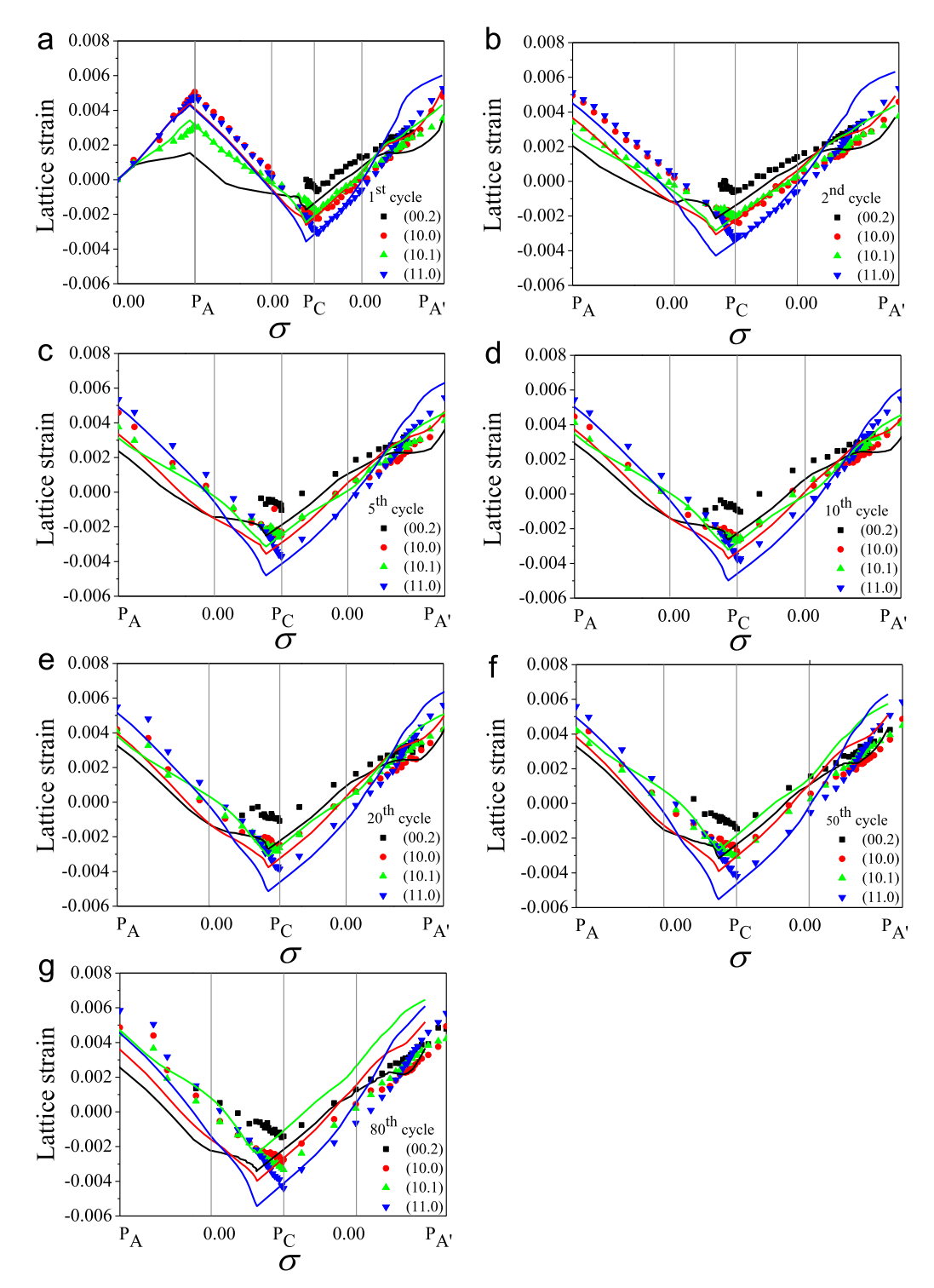


Fig. 8. Experimental (solid and open symbols) and predicted (solid lines) lattice strains as a function of stress for different cycles of the AZ31 plate.

Nevertheless, the research by Hazeli et al. (2015) demonstrates that not only a portion of twins can de-twin or continue growth at reverse tension. This reversible twinning is active even at the three quarters of the whole fatigue life. Similar results have been researched by Yu et al. (2011). This indicates that the saturation of twinning does not appear at early stage of fatigue. It is also established that the residual twins at each circle gradually increase with fatigue cycle (Wu et al., 2008).

Benefiting from a good modeling to the whole fatigue life, the results in the present study can provide more details about the

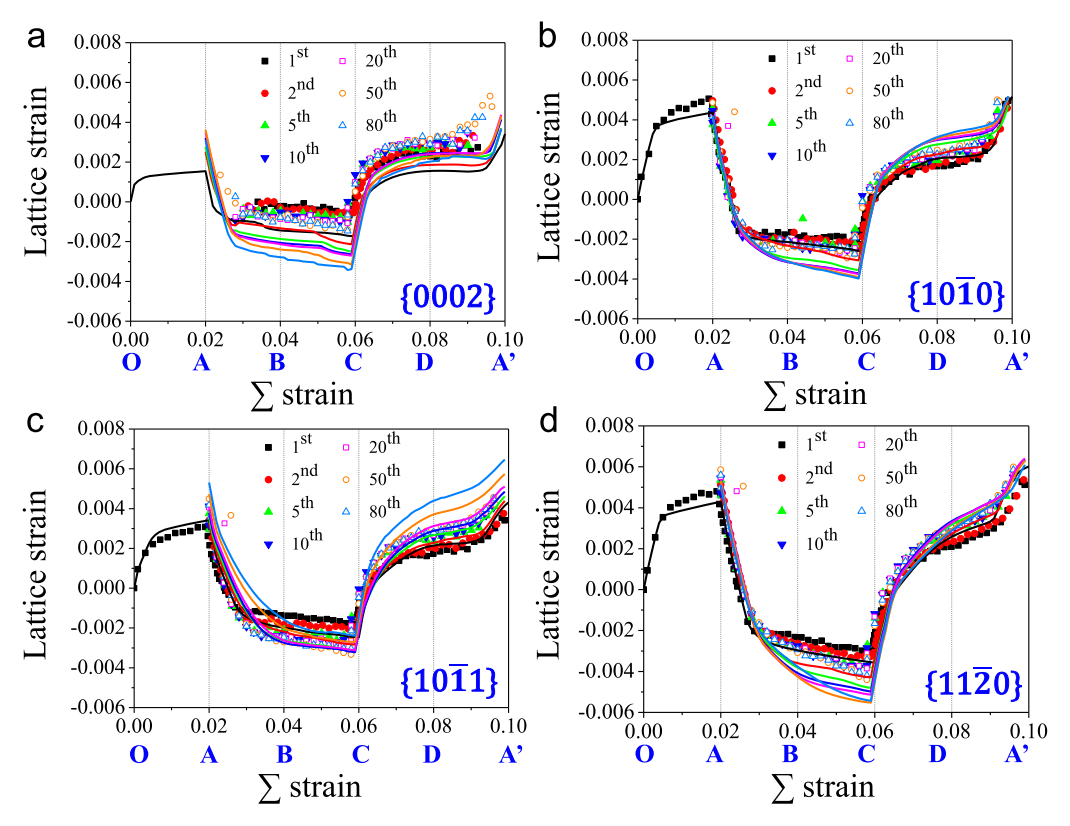


Fig. 9. Measured (solid and open symbols) and predicted (solid lines) lattice strains as a function of strain for different cycles of the AZ31 plate.

evolution of twinning-detwinning behavior with fatigue cycle. As discussed in the prior section, it is widely considered that the maximum twin volume fraction for each cycle increases initially, and then tends to be saturated (Yin et al., 2008a, 2008b; Park et al., 2010,2016; Lv et al., 2011a, 2011b). However, the simulations and the results of neutron diffraction in the present study clearly show that the maximum twin volume fraction (Point C) of each cycle is found to: first increases (1st to 2nd cycle), then decreases (2nd to 20th cycle), and increases again (20th to 80th cycle). Although there is a small difference for the critical cycle for this transition between simulations and neutron diffraction, the two results indicate a similar trend. Such a trend has not been reported previously. The reasons for the variation of the maximum twin volume fraction with fatigue cycle can be explained by the relative activities of twinning and slips in Fig. 11. Obviously, the twin volume fraction during low-cycle fatigue is mainly determined by the activity of $\{10\overline{1}2\}$ twinning and the volume fraction of residual twins. There is a high volume fraction of residual twins after the 1st cycle, as shown in Fig. 6. Therefore, the increase of the maximum twin volume fraction from 1st to 2nd cycle is probably due to a high fraction of residual twins after the 1st cycle. After the 1st cycle, the relative activity of the basal slip increases, and that of $\{10\overline{1}2\}$ twinning decreases (Figs. 10 and 11). A lower activity of twinning will lead to a lower twin volume fraction after a certain cycle. Meanwhile, the contribution of residual twins is not significant at this stage. Therefore, the subsequent decrease of twin volume fraction can be ascribed to the gradually-decreased relative activity of $\{10\overline{1}2\}$ twinning and the marginal increase of residual twins. It is well established that both twinning and detwinning will become more difficult with an increase of the dislocations within material at the late stage, which results in a quick increase of residual twins. Similar behaviors have been observed in several other studies (Cáceres et al., 2003; Brown et al., 2007). As a result, the secondary increase of the maximum twins after the 20th cycle is mainly related to a quick increase of residual twins. In a previous research, Dong et al. (2015) reported that an enhanced nucleation sites of twins were responsible for an increased twin volume fraction with fatigue cycle. However, the twin volume fraction is in connection with both twin nucleation and twin growth. The enhancement of twin nucleation does not necessarily lead to an increase of twin volume fraction. The above discussions indicate that a good model of detwinning is very important to simulate both the twinning behavior and the residual twins during low-cycle fatigue of Mg alloys. Previous models often do not contain detwinning mechanism, leading to an inaccurate calculation for twinning and residual twins.

It is worth mentioning that the simulations in the present investigation show that the twin volume fraction decreases to 7.5% rather than 0 during the reverse loading to tension at the first cycle (see Fig. 6), which indicates that the residual twins appear at the first cycle, and are even high to 7.5%. This trend is different from the result of neutron diffraction with a very small fraction of residual twins at the 1st cycle. This feature means that the detwinning in this model is slightly undervalued. A possible reason is that the CRSS for detwinning used in the simulations is higher than that of basal slip. Another reason is probably related to that the fraction of residual twins at early stage is too small to be detected by neutron diffraction. As demonstrated in Section 3.4, a small fraction of

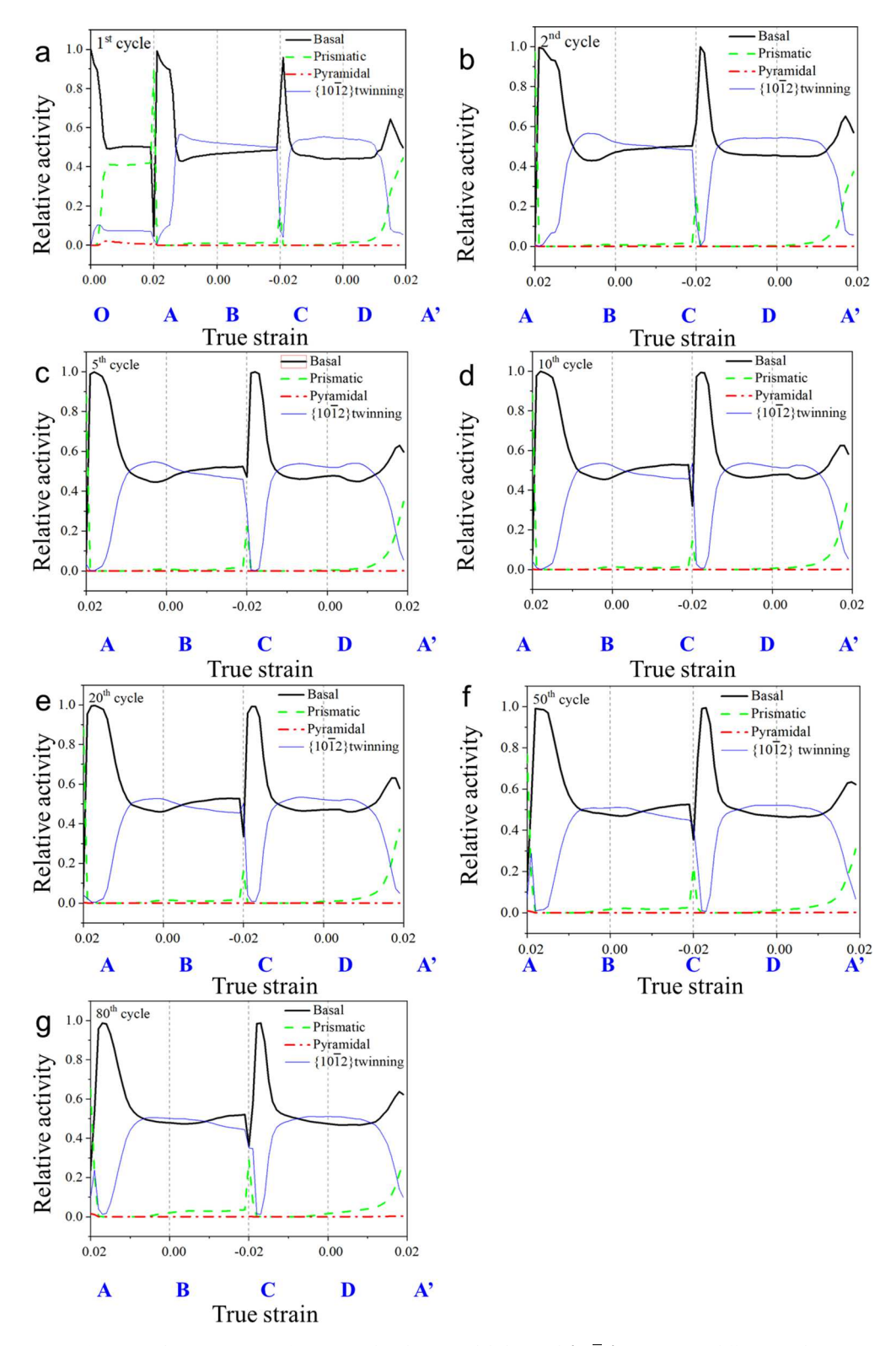


Fig. 10. Relative activities of prismatic, basal, pyramidal slips and $\{10\overline{1}2\}$ twinning at different cycles.

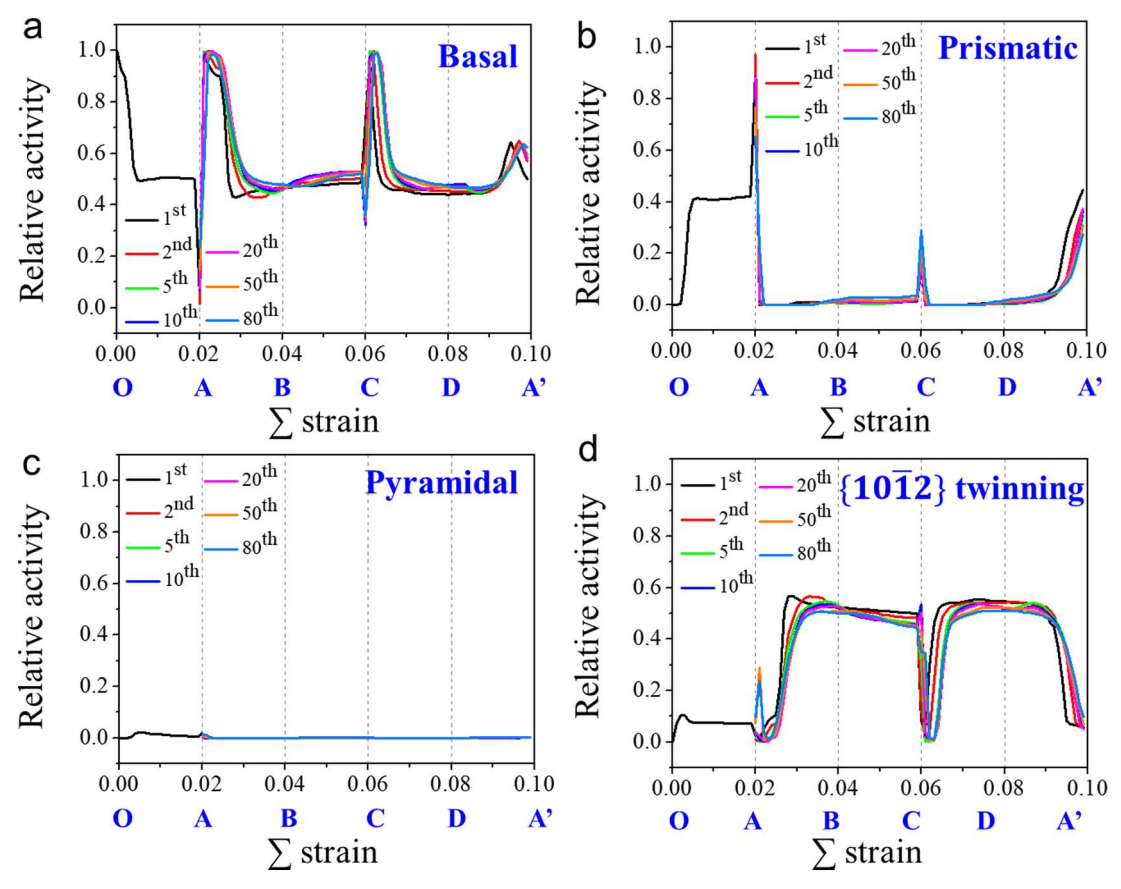


Fig. 11. Evolution of the relative activities for different deformation mechanisms with the increase of fatigue cycles: (a) basal slip; (b) prismatic slip; (c) pyramidal slip; (d) $\{10\overline{1}2\}$ twinning.

twinning takes place during the initial tension of the 1st cycle, which is confirmed by both the simulations and neutron diffraction. For a hot-rolled plate, basal poles are largely parallel to the ND (Koike, 2005). This type of orientation does not favor $\{10\overline{1}2\}$ twinning under tension along the RD (Yu et al., 2017). Nevertheless, there is also a small fraction of grains with their c-axis inclining largely from the ND, and $\{10\overline{1}2\}$ twins might appear in those grains during the initial tension.

4.2. Evolution of the peak stress

The evolution of mechanical response with fatigue cycle is an important issue in fatigue process. As shown in Fig. 4, an obvious hardening of the peak stress appears: the peak stress at tension stage marginally increases in the first 10 cycles, and afterward, becomes saturated, while the peak stress for compression stage keeps rising throughout the whole fatigue life. Such a cyclic-stress response can be ascribed to a stability or variation of microstructural features. Previously, the mechanisms for cyclic hardening of the peak stress have been discussed in several studies (Barnett et al., 2004; Begum et al., 2009; Wu et al., 2010b), and are mainly ascribed to the following factors. First, the cyclic hardening results from the multiplication of dislocations. Second, twin can transform glissile dislocations into sessile ones to impede dislocation slip. Third, residual twins can act as barriers against dislocation slip. All these factors might contribute to a cyclic hardening under high strain amplitudes (Barnett et al., 2004; Begum et al., 2009; Wu et al., 2010b; Geng et al., 2013). However, these reasons are so general that it is insufficient to explain some specific phenomena. For example, why the compressive peak stress in the first 10 cycles increases faster than that after the 10th cycle in the current investigation; why the cyclic hardening of tensile stress is evidently lower than that for compressive stress.

Previously, some researchers considered that the cyclic hardening of compressive peak stress was due to an increase in twin volume fraction (Wu et al., 2008, 2010a; Hama et al., 2012). For example, Wu et al. (2008) held that the increase of twin volume fraction could account for the hardening of the compressive peak stress. In addition, Park et al. (2010) thought that the rising volume fraction of residual twins with fatigue cycles would become barriers against dislocation slip, mainly accounting for the cyclic hardening of compression peak stress. Nevertheless, the results in the present study show that the twin volume fraction firstly increases before the 10th cycle, followed by decreasing, and re-increasing after the 20th cycle. Therefore, it cannot simply conclude that the cyclic hardening of compressive peak stress is related to an increase of twin volume fraction with fatigue cycles. The volume fraction of residual twins increases during the whole fatigue life, and rises faster at the later stage. That is, the compressive peak stress should not

be saturated after 10 cycles, and exhibits a faster hardening rate. Evidently, this deduction contradicts with the experimental observations. The results in Fig. 9 allow a reasonable explanation for the evolution of cyclic hardening of compressive peak stress. $\{10\overline{1}2\}$ twinning dominates the plastic-deformation stage of compression. The gliding dislocations due to basal/non-basal slips and residual twin dislocations after repeated twinning-detwinning process can multiply and accumulate with loading cycles. Certain irreversible dislocation substructures and residual twins can stabilize twin boundaries, making twinning more difficult (Dong et al., 2015, 2017). This trend will increase the compressive peak stress. Therefore, the hardening of compressive peak stress is related mainly to the strong interactions of $\{10\overline{1}2\}$ twinning with previously-stored deformation substructures. The results in Fig. 10 show that the maximum lattice strains of the $\{11\overline{2}0\}$ and $\{10\overline{1}0\}$ at Point C increase quickly during the first 10 cycles and very slow after 10 cycles. This trend indicates that the barrier effect to twinning is very pronounced during the early cycles, but is effectively weakened at the later cycles. Therefore, the much lower hardening rate after 10 cycles is related to a gradually-decreased barrier effect against twinning.

Previously, the reasons for the cyclic hardening of tensile peak stress were widely ascribed to dislocation-dislocation interactions. This feature can also be confirmed from the deformation behavior of simulations. At the initial stage of tension, detwinning is the predominant mode to accommodate plastic deformation. And prismatic slip was very important when the detwinning is exhausted. Hence, the cyclic hardening of tensile peak stress can be ascribed to an increase of the amount of dislocations and the interactions between prismatic slip and residual deformation structures . It can be seen in Fig. 4 that there is a much stronger cyclic-hardening response of compressive peak stress than tensile peak stress. This should be ascribed to the fact that the residual twins and dislocations during cyclic loading generate a higher hardening on $\{10\overline{1}2\}$ twinning than on prismatic slip.

5. Conclusions

The simulations using EVPSC-TDT model and the real-time *in-situ* neutron-diffraction technique under a continuous loading condition were employed to study the low-cycle fatigue behavior of the wrought AZ31B Mg alloy. The relationship between the deformation behavior and mechanical response was discussed. The main conclusions are reached as follows:

- (1) Previous models and simulations cannot simultaneously reproduce well the mechanical response and twinning-detwinning behavior during a low cycle fatigue loading, in particular for high strain amplitudes. Both the mechanical response and twinning-detwinning behavior throughout the whole fatigue life (80 cycles) are well predicted by the EVPSC-TDT model in the present study. The simulations well reproduce the hysteresis loops and cyclic-hardening response from the 1st to 80th cycle. The predicted evolutions of the maximum twin volume fraction and residual twins exhibit similar trends to those measured by *in-situ* neutron diffraction. For the first time, the evolution of lattice strain throughout the whole fatigue life is simulated, which is in good accordance with that determined by neutron diffraction.
- (2) Combining the results of simulations and neutron diffraction, new understandings on the twinning-detwinning behavior throughout the whole fatigue life are achieved. It is found that the evolution of the maximum twin volume fraction of each cycle shows an increase from the 1st to 2nd cycle, followed by a decrease from the 2nd to 20th cycle, and a secondary increase after the 20th cycle. This finding corrects the previous opinion that the maximum twin fraction increases at the initial stage, and tends to be saturated at the late stage. The first increase of the maximum twin fraction from the 1st to 2nd cycle is mainly related to a high fraction of residual twins after the 1st cycle. The subsequent decrease from the 2nd to 20th cycle is ascribed mainly to a decreasing activity of $\{10\overline{1}2\}$ twinning and the marginal increase of residual twins. After the 20th cycle, the fraction of residual twins exhibits a quick increase, resulting in a secondary increase of the maximum twin volume fraction.
- (3) Some new insights on the mechanisms for cyclic hardening are provided. The cyclic hardening at compression stage comes from mainly the stabilization of $\{10\overline{1}2\}$ twin boundary by the irreversible dislocation substructures and residual twins generated in previous cycles. In contrast, the interaction between prismatic slip and the residual deformation substructures mainly accounts for the cyclic hardening at tensile stage. A higher hardening on the prismatic slip than on the $\{10\overline{1}2\}$ twinning would lead to a stronger cyclic hardening response of compressive peak stress than tensile peak stress.

CRediT authorship contribution statement

Xiaoqian Guo: Investigation, Writing – original draft, Writing – review & editing, Visualization. Yao Cheng: Investigation, Data curation, Writing – original draft, Writing – review & editing, Visualization. Yunchang Xin: Conceptualization, Validation, Supervision, Formal analysis, Writing – original draft, Writing – review & editing, Project administration, Funding acquisition. Wei Wu: Investigation, Data curation, Visualization. Chao Ma: Formal analysis. Ke An: Investigation, Data curation, Visualization. Peter K. Liaw: Investigation, Data curation, Funding acquisition. Peidong Wu: Methodology, Writing – review & editing, Supervision. Qing Liu: Supervision, Funding acquisition.

Declaration of Competing Interest

The authors declare that they have no known competing financial interests or personal relationships that could have appeared to influence the work reported in this paper.

Acknowledgments

X.Q. Guo acknowledges the support of the National Natural Science Foundation of China (51601218), Project funded by the China Postdoctoral Science Foundation (2020M671640) and Project supported by the Key Laboratory of Lightweight Materials. C. Ma acknowledges the support of the Natural Science Foundation of the Jiangsu Province (BK20200172) and the Natural Science Foundation of the Jiangsu Higher Education Institutions of China (19KJB430037). Y.C. Xin was supported by the Natural Science Foundation of Jiangsu Province (BK20202010). P. K. Liaw very much appreciates the supports from the National Science Foundation (DMR-1611180 and 1809640) with program directors, Drs. J. Yang, G. Shiflet, and D. Farkas and the US Army Research Office (W911NF-13-1-0438 and W911NF-19-2-0049) with program managers, Drs. M.P. Bakas, S.N. Mathaudhu, and D.M. Stepp. P.D. Wu was supported by the Natural Science and Engineering Research Council of Canada (RGPIN-2016-06464).

References

- Agnew, S.R., Brown, D.W., Tomé, C.N., 2006. Validating a polycrystal model for the elastoplastic response of magnesium alloy AZ31 using *in situ* neutron diffraction. Acta Mater. 54. 4841–4852.
- Agnew, S.R., Tomé, C.N., Brown, D.W., Holden, T.M., Vogel, S.C., 2003. Study of slip mechanisms in a magnesium alloy by neutron diffraction and modeling. Scr. Mater. 48, 1003–1008.
- Barnett, M.R., Keshavarz, Z., Beer, A.G., Atwell, D., 2004. Influence of grain size on the compressive deformation of wrought Mg-3Al-1Zn. Acta Mater 52, 5093–5103. Begum, S., Chen, D.L., Xu, S., Luo, A.A., 2009. Low cycle fatigue properties of an extruded AZ31 magnesium alloy. Int. J. Fatigue 31, 726–735.
- Briffod, F., Shiraiwa, T., Enoki, M., 2019. Numerical investigation of the influence of twinning/detwinning on fatigue crack initiation in AZ31 magnesium alloy. Mater. Sci. Eng. A 753, 79–90.
- Briffod, F., Shiraiwa, T., Enoki, M., 2020. Monotonic and cyclic anisotropies of an extruded Mg-Al-Ca-Mn alloy plate: experiments and crystal plasticity studies. Mater. Sci. Eng. A 772, 12.
- Brown, D.W., Jain, A., Agnew, S.R., Clausen, B., Chandra, T., Tsuzaki, K., Militzer, M., Ravindran, C., 2007. Twinning and detwinning during cyclic deformation of Mg alloy AZ31B. Thermec 2006. Trans Tech Publications, Switzerland, pp. 3407–3413.
- Cáceres, C.H., Sumitomo, T., Veidt, M., 2003. Pseudoelastic behaviour of cast magnesium AZ91 alloy under cyclic loading-unloading. Acta Mater. 51, 6211–6218. Chen, C., Liu, T., Lv, C., Lu, L., Luo, D., 2012. Study on cyclic deformation behavior of extruded Mg-3Al-1Zn alloy. Mater. Sci. Eng. A 539, 223–229.
- Chen, Y., Hu, G.J., Lan, Y.T., Zhang, K.S., Cai, G.W., 2018. Constitutive modeling of slip, twinning and detwinning for Mg alloy and inhomogeneous evolution of microstructure. Acta Mech. Solida Sin. 31, 493–511.
- Dong, S., Yu, Q., Jiang, Y., Dong, J., Wang, F., Ding, W., 2015. Electron backscatter diffraction observations of twinning-detwinning evolution in a magnesium alloy subjected to large strain amplitude cyclic loading. Mater. Des. 65, 762–765.
- Dong, S., Yu, Q., Jiang, Y., Dong, J., Wang, F., Jin, L., Ding, W., 2017. Characteristic cyclic plastic deformation in ZK60 magnesium alloy. Int. J. Plast. 91, 25–47. Duan, G.S., Wu, B.L., Du, X.H., Zhao, X., Zhang, Y.D., Zuo, L., Esling, C., 2014. The cyclic frequency sensitivity of low cycle fatigue (LCF) behavior of the AZ31B magnesium alloy. Mater. Sci. Eng. A 603, 11–22.
- Geng, C.J., Wu, B.L., Du, X.H., Wang, Y.D., Zhang, Y.D., Wagner, F., Esling, C., 2013. Low cycle fatigue behavior of the textured AZ31B magnesium alloy under the asymmetrical loading. Mater. Sci. Eng. A 560, 618–626.
- Gu, C., Toth, L., 2012. Polycrystal modeling of tensile twinning in a Mg alloy during cyclic loading. Scr. Mater. 67, 673-676.
- Gu, C.F., Toth, L.S., Hoffman, M., 2014. Twinning effects in a polycrystalline magnesium alloy under cyclic deformation. Acta Mater. 62, 212–224.
- Guillemer, C., Clavel, M., Cailletaud, G., 2011. Cyclic behavior of extruded magnesium: experimental, microstructural and numerical approach. Int. J. Plast. 27, 2068–2084.
- Guo, X.Q., Chapuis, A., Wu, P.D., Agnew, S.R., 2015. On twinning and anisotropy in rolled Mg alloy AZ31 under uniaxial compression. Int. J. Solids Struct. 64-65, 42-50.
- Hama, T., Kariyazaki, Y., Hosokawa, N., Fujimoto, H., Takuda, H., 2012. Work-hardening behaviors of magnesium alloy sheet during in-plane cyclic loading. Mater. Sci. Eng. A 551, 209–217.
- Hazeli, K., Askari, H., Cuadra, J., Streller, F., Carpick, R.W., Zbib, H.M., Kontsos, A., 2015. Microstructure-sensitive investigation of magnesium alloy fatigue. Int. J. Plast. 68, 55–76.
- Hong, S.G., Park, S.H., Lee, C.S., 2011. Enhancing the fatigue property of rolled AZ31 magnesium alloy by controlling {10-12} twinning-detwinning characteristics. J. Mater. Res. 25, 784–792.
- Kang, G., Li, H., 2021. Review on cyclic plasticity of magnesium alloys: experiments and constitutive models. Int. J. Miner. Met. Mater. 28, 567-589.
- Karparvarfard, S.M.H., Shaha, S.K., Behravesh, S.B., Jahed, H., Williams, B.W., 2019. Fatigue characteristics and modeling of cast and cast-forged ZK60 magnesium alloy. Int. J. Fatigue 118, 282–297.
- Knezevic, M., Levinson, A., Harris, R., Mishra, R.K., Doherty, R.D., Kalidindi, S.R., 2010. Deformation twinning in AZ31: influence on strain hardening and texture evolution. Acta Mater. 58, 6230–6242.
- Koike, J., 2005. Enhanced deformation mechanisms by anisotropic plasticity in polycrystalline Mg alloys at room temperature. Metall. Mater. Trans. A 36, 1689–1696. Koike, J., Fujiyama, N., Ando, D., Sutou, Y., 2010. Roles of deformation twinning and dislocation slip in the fatigue failure mechanism of AZ31 Mg alloys. Scr. Mater. 63, 747–750.
- Kulekci, M.K., 2008. Magnesium and its alloys applications in automotive industry. Int. J. Adv. Manuf. Technol. 39, 851-865.
- Kwon, S.H., Song, K.S., Shin, K.S., Kwun, S.I., 2011. Low cycle fatigue properties and an energy-based approach for as-extruded AZ31 magnesium alloy. Met. Mater. Int. 17, 207–213.
- Lei, Y., Wang, Z., Kang, G., 2022. Experimental investigation on uniaxial cyclic plasticity of cast AZ91 magnesium alloy. J. Magnes. Alloy. In press.
- Li, H., Kang, G., Yu, C., 2020. Modeling uniaxial ratchetting of magnesium alloys by a new crystal plasticity considering dislocation slipping, twinning and detwinning mechanisms. Int. J. Mech. Sci. 179, 105660.
- Li, H., Yu, C., Kang, G., 2022. Crystal plasticity modeling of the multiaxial ratchetting of extruded AZ31 Mg alloy. Int. J. Plast. 152, 103242.
- Lv, F., Yang, F., Duan, Q.Q., Yang, Y.S., Wu, S.D., Li, S.X., Zhang, Z.F., 2011a. Fatigue properties of rolled magnesium alloy (AZ31) sheet: influence of specimen orientation. Int. J. Fatigue 33, 672–682.
- Lv, F., Yang, F., Li, S.X., Zhang, Z.F., 2011b. Effects of hysteresis energy and mean stress on low-cycle fatigue behaviors of an extruded magnesium alloy. Scr. Mater. 65, 53–56.
- Ma, C., Chapuis, A., Guo, X.Q., Zhao, L.Y., Wu, P.D., Liu, Q., Mao, X.B., 2017. Modeling the deformation behavior of a rolled Mg alloy with the EVPSC-TDT model. Mater. Sci. Eng. A 682, 332–340.
- Ma, C., Wang, H.M., Hama, T., Guo, X.Q., Mao, X.B., Wange, J., Wu, P., 2019. Twinning and detwinning behaviors of commercially pure titanium sheets. Int. J. Plast. 121, 261–279.
- Matsuzuki, M., Horibe, S., 2009. Analysis of fatigue damage process in magnesium alloy AZ31. Mater. Sci. Eng. A 504, 169–174.
- Mokdad, F., Chen, D.L., 2015. Strain-controlled low cycle fatigue properties of a rare-earth containing ZEK100 magnesium alloy. Mater. Des. 67, 436–447.
- Murphy-Leonard, A.D., Pagan, D.C., Beaudoin, A., Miller, M.P., Allison, J.E., 2019. Quantification of cyclic twinning-detwinning behavior during low-cycle fatigue of pure magnesium using high energy X-ray diffraction. Int. J. Fatigue 125, 314–323.

- Park, S.H., Hong, S.G., Bang, W., Lee, C.S., 2010. Effect of anisotropy on the low-cycle fatigue behavior of rolled AZ31 magnesium alloy. Mater. Sci. Eng. A 527, 417-423
- Park, S.H., Hong, S.G., Yoon, J., Lee, C.S., 2016. Influence of loading direction on the anisotropic fatigue properties of rolled magnesium alloy. Int. J. Fatigue 87, 210–215
- Qiao, H., Agnew, S.R., Wu, P.D., 2015a. Modeling twinning and detwinning behavior of Mg alloy ZK60A during monotonic and cyclic loading. Int. J. Plast. 65, 61–84. Qiao, H., Barnett, M.R., Wu, P.D., 2016a. Modeling of twin formation, propagation and growth in a Mg single crystal based on crystal plasticity finite element method. Int. J. Plast. 86, 70–92.
- Qiao, H., Guo, X.Q., Hong, S.G., Wu, P.D., 2017a. Modeling of {10-12}-{10-12} secondary twinning in pre-compressed Mg alloy AZ31. J. Alloy. Compd. 725, 96–107. Qiao, H., Guo, X.Q., Oppedal, A.L., El Kadiri, H., Wu, P.D., Agnew, S.R., 2017b. Twin-induced hardening in extruded Mg alloy AM30. Mater. Sci. Eng. A 687, 17–27.
- Qiao, H., Wu, P.D., Guo, X.Q., Agnew, S.R., 2016b. A new empirical equation for termination of twinning in magnesium alloys. Scr. Mater 120, 71–75. Qiao, H., Wu, P.D., Wang, H., Gharghouri, M.A., Daymond, M.R., 2015b. Evaluation of elastic-viscoplastic self-consistent polycrystal plasticity models for zirconium alloys. Int. J. Solids Struct. 71, 308–322.
- Simmons, G., Wang, H., 1971. Single Crystal Elastic Constants and Calculated Aggregate Properties: A Handbook, 2nd ed. MIT Press, Cambridge.
- Singh, J., Kim, M.S., Kaushik, L., Kang, J.H., Kim, D., Martin, E., Choi, S.H., 2020. Twinning-detwinning behavior of E-form Mg alloy sheets during in-plane reverse loading. Int. J. Plast. 127, 21.
- Song, L.H., Wu, B.L., Zhang, L., Du, X.H., Wang, Y.N., Zhang, Y.D., Esling, C., 2017. Cyclic deformation behaviors of AZ31B magnesium alloy in two different asymmetric loading manners. Mater. Sci. Eng. A 689, 134–141.
- Wang, H., Raeisinia, B., Wu, P.D., Agnew, S.R., Tome, C.N., 2010a. Evaluation of self-consistent polycrystal plasticity models for magnesium alloy AZ31B sheet. Int. J. Solids Struct. 47, 2905–2917.
- Wang, H., Wu, P., Wang, J., 2015a. Numerical assessment of the role of slip and twinning in magnesium alloy AZ31B during loading path reversal. Metall. Mater. Trans. A 46, 3079–3090.
- Wang, H., Wu, P.D., Tome, C.N., Huang, Y., 2010b. A finite strain elastic-viscoplastic self-consistent model for polycrystalline materials. J. Mech. Phys. Solids 58, 594–612.
- Wang, H., Wu, P.D., Tome, C.N., Wang, J., 2012a. Study of lattice strains in magnesium alloy AZ31 based on a large strain elastic-viscoplastic self-consistent polycrystal model. Int. J. Solids Struct. 49, 2155–2167.
- Wang, H., Wu, P.D., Tomé, C.N., Wang, J., 2012b. A constitutive model of twinning and detwinning for hexagonal close packed polycrystals. Mater. Sci. Eng. A 555, 93–98.
- Wang, H., Wu, P.D., Wang, J., 2015b. Modelling the role of slips and twins in magnesium alloys under cyclic shear. Comput. Mater. Sci. 96, 214–218. Wang, H., Wu, P.D., Wang, J., Tomé, C., 2013. A physics-based crystal plasticity model for hexagonal close packed (HCP) crystals including both twinning and
- detwinning mechanisms. Int. J. Plast. 49, 2155–2167.
 Wang, X.L., Holden, T.M., Rennich, G.Q., Stoica, A.D., Liaw, P.K., Choo, H., Hubbard, C.R., 2006. VULCAN-the engineering diffractometer at the SNS. Phys. B Condens. Matter 385-386. 673–675.
- Wang, Y., Culbertson, D., Jiang, Y., 2020. An experimental study of anisotropic fatigue behavior of rolled AZ31B magnesium alloy. Mater. Des. 186, 108266. Wu, L., Agnew, S.R., Ren, Y., Brown, D.W., Clausen, B., Stoica, G.M., Wenk, H.R., Liaw, P.K., 2010a. The effects of texture and extension twinning on the low-cycle
- fatigue behavior of a rolled magnesium alloy, AZ31B. Mater. Sci. Eng. A 527, 7057–7067.

 Wu, L., Jain, A., Brown, D.W., Stoica, G.M., Agnew, S.R., Clausen, B., Fielden, D.E., Liaw, P.K., 2008. Twinning-detwinning behavior during the strain-controlled low-cycle fatigue testing of a wrought magnesium alloy, ZK60A. Acta Mater. 56, 688–695.
- Wu, W., Liaw, P.K., An, K., 2015. Unraveling cyclic deformation mechanisms of a rolled magnesium alloy using in situ neutron diffraction. Acta Mater. 85, 343–353.
- Wu, W., Qiao, H., An, K., Guo, X., Wu, P., Liaw, P.K., 2014. Investigation of deformation dynamics in a wrought magnesium alloy. Int. J. Plast. 62, 105–120.
- Wu, Y.J., Zhu, R., Wang, J.T., Ji, W.Q., 2010b. Role of twinning and slip in cyclic deformation of extruded Mg-3%Al-1%Zn alloys. Scr. Mater. 63, 1077-1080.
- Yaghoobi, M., Allison, J.E., Sundararaghavan, V., 2020. Multiscale modeling of twinning and detwinning behavior of HCP polycrystals. Int. J. Plast. 127, 102653. Yin, S.M., Yang, F., Yang, X.M., Wu, S.D., Li, S.X., Li, G.Y., 2008a. The role of twinning-detwinning on fatigue fracture morphology of Mg-3%Al-1%Zn alloy. Mater. Sci. Eng. A 494, 397–400.
- Yin, S.M., Yang, H.J., Li, S.X., Wu, S.D., Yang, F., 2008b. Cyclic deformation behavior of as-extruded Mg-3%Al-1%Zn. Scr. Mater. 58, 751-754.
- Yu, C., Kang, G., Kan, Q., 2014. Crystal plasticity based constitutive model for uniaxial ratchetting of polycrystalline magnesium alloy. Comput. Mater. Sci. 84, 63–73. Yu, H.H., Li, C.Z., Xin, Y.C., Chapuis, A., Huang, X.X., Liu, Q., 2017. The mechanism for the high dependence of the Hall-Petch slope for twinning/slip on texture in Mg alloys. Acta Mater. 128, 313–326.
- Yu, Q., Zhang, J., Jiang, Y., 2011. Direct observation of twinning-detwinning on magnesium single crystal subjected to strain-controlled cyclic tension-compression in 0001 direction. Philos. Mag. Lett. 91, 757–765.
- Yu, Q., Zhang, J., Jiang, Y., Li, Q., 2012. An experimental study on cyclic deformation and fatigue of extruded ZK60 magnesium alloy. Int. J. Fatigue 36, 47–58. Yu, Q., Wang, J., Jiang, Y., 2013. Inverse slip accompanying twinning and detwinning during cyclic loading of magnesium single crystal. J. Mater. 2013, 903786.
- Tal, Q., Wang, Y., Shang, Y., Shang, Y., Shang, Y., Shang, Y., Shang, Y., Shang, H., Jérusalem, A., Salvati, E., Papadaki, C., Fong, K.S., Song, X., Korsunsky, A.M., 2019. Multi-scale mechanisms of twinning-detwinning in magnesium alloy AZ31B simulated by crystal plasticity modeling and validated via in situ synchrotron XRD and in situ SEM-EBSD. Int. J. Plast. 119, 43–56.
- Zhang, J., Yu, Q., Jiang, Y., Li, Q., 2011. An experimental study of cyclic deformation of extruded AZ61A magnesium alloy. Int. J. Plast. 27, 768–787.
- Zhang, M., Zhang, H., Ma, A., Llorca, J., 2021a. Experimental and numerical analysis of cyclic deformation and fatigue behavior of a Mg-RE alloy. Int. J. Plast. 139, 102885
- Zhang, N.B., Zhang, Y.Y., Chen, S., Zhang, B.B., Li, Z.L., Xie, H.L., Lu, L., Yao, X.H., Luo, S.N., 2021b. Onset of detwinning in Mg-3Al-1Zn alloy: a synchrotron-based X-ray diffraction study. Scr. Mater. 190, 113–117.
- Zhao, L., Guo, X., Chapuis, A., Xin, Y., Liu, Q., Wu, P., 2019. Strain-path dependence of {10-12}twinning in a rolled Mg-3Al-1Zn alloy: influence of twinning model. Metall. Mater. Trans. A 50, 118–131.